Structural studies of apatite-type oxide ion conductors doped with Cobalt

Julian R. Tolchard, Jonathan E.H. Sansom, M. Saiful Islam, and Peter R. Slater*

Chemistry, SBMS, University of Surrey, Guildford, GU2 7XH, UK

*Corresponding Author

Dr P.R. Slater

Chemistry, SBMS

University of Surrey

Guildford GU2 7XH.

UK

Tel: +44-1483-686847

Fax: +44-1483-686851

Email: p.slater@surrey.ac.uk

Abstract

A series of Co doped lanthanum silicate apatite-type phases, $La_{9.83}Si_{4.5}Co_{1.5}O_{26}$, $La_{9.66}Si_5CoO_{26,}$ $La_{10}Si_5CoO_{26.5}$ and $La_8BaCoSi_6O_{26}$, have been synthesised, and neutron diffraction, EXAFS and XANES used to investigate their structures in detail. All compositions were shown to possess the hexagonal apatite structure, and the results confirmed that cobalt can be doped onto both the La and Si sites within the structure depending on the starting composition. The Co doping is shown to cause considerable local distortions within the apatite structure. In the case of Si site doping two compositions showed anisotropic peak broadening, which has been attributed to incommensurate ordering of oxygen within the apatite channels.

Keywords: apatite, solid oxide fuel cell, ionic conductor, neutron diffraction, EXAFS, XANES

1. Introduction

Fast oxygen ion conductors are an increasingly important class of materials, with wide ranging applications in sensors, gas separation membranes and Solid Oxide Fuel Cells (SOFCs). The latter is the focus of much recent research, as the high efficiency and ability of SOFCs to act as a bridging technology between hydrocarbon and hydrogen fuel technologies makes them prime candidates for next generation power production.

Apatite materials, particularly the rare earth silicate and germanate systems, are attracting great interest as a new class of oxygen anion conductor [1-20] . With high conductivities at intermediate temperatures (> 10^{-3} Scm^{-1} at 500ºC for a range of compositions), they are of particular interest as SOFC materials, potentially offering the opportunity to reduce the fuel cell operating temperature to a point where less costly materials can be utilised in the SOFC construction.

Isostructural with the well known Apatite mineral group, these materials take the general formula $M_{10}(XO_4)_6O_{2\pm y}$, where M is a metal such as a rare earth or alkaline earth and X is a p-block element such as P, Si, Ge. With such a wide range of substitutional possibilities, there is great potential for optimising these materials' properties. The structure (figure 1) comprises isolated XO_4 tetrahedra arranged so as to form two distinct channels running along the c-direction. Occupying the smaller of these channels are M cations, whilst the larger channel contains a "ring" of M cations with oxygen anions occupying positions in the channel centre.

Studies have shown that conduction in these systems is wholly anionic [1,3] , with high oxygen transference numbers (>0.9) across a wide range of oxygen partial pressures. Single crystal studies [4,5] on Nd analogues have shown that this conduction is anisotropic, favouring the c-direction. It has also been observed that cation doping regimes and non-stoichiometry can significantly influence conductivity. In particular, it has been found that fully stoichiometric systems, such as $La_8Sr_2Si_6O_{26}$ exhibit generally poor conductivities, whilst samples containing cation vacancies at the ±(2/3,1/3,z) sites show markedly improved conductivities, particularly if aliovalent cations, such as Ga^{3+}, Al^{3+}, have been doped onto the Si site, e.g. $La_{9.83}Si_{4.5}M_{1.5}O_{26}$ (M=Al, Ga) [1,6-10]. The highest conductivities, however, are found for the oxygen excess samples, e.g. $La_9MSi_6O_{26.5}$ (M=Ca, Sr, Ba) [2,3,11]. It has therefore been suggested that conduction occurs along the [0,0,z] channel and goes via oxygen interstitials, an implication strengthened by neutron diffraction studies of the $La_{9.33}M_6O_{26}$ (where M=Si, Ge) systems [6,12] in which the high conductivities were found to be linked to a large degree of observed anion disorder along the [0,0,z] channels.

Recent computer simulation studies of the $La_{9.33}Si_6O_{26}$ and $La_8Sr_2Si_6O_{26}$ systems [13],[14] support these observations, predicting an interstitial conduction mechanism along the [0,0,z] channels to be energetically favoured. Additionally a low energy interstitial position was predicted to exist, lying close to the SiO_4 substructure on the periphery of the [0,0,z] channels. Further experimental studies have provided confirmation of this position, with Leon-Reina et al [15] showing occupation of a similar site in neutron diffraction studies of the $La_{9.55}Si_6O_{26.32}$, $La_{9.6}Si_6O_{26.34}$ and $La_{9.60}Ge_6O_{26.4}$ systems, and

Kharton et al [16] reporting penta-coordinated Fe^{3+} in Mössbauer studies of $La_{10}Si_5FeO_{26.5}$.

The understanding of the conductivity in these systems is still, however, incomplete. In particular, the role of cation dopants and the observed oxygen disorder are only now becoming better understood through modelling and neutron diffraction studies. In this work previous studies on Co doping [7] are extended to investigate the structural effects of doping cobalt onto both the La and Si sites of the lanthanum silicate systems via the complementary use of high resolution neutron diffraction and X-ray Absorption Spectroscopy (EXAFS), so as to provide a detailed structural picture of the effect of Co doping. The results highlight the structural complexities of these apatite systems as well as their flexibility regarding cation doping on the La and Si sites.

2. Experimental

A selection of Co-containing samples were prepared with Co on either the Si site, $La_{9.83}Si_{4.5}Co_{1.5}Co_{1.5}O_{26}$, $La_{9.66}Si_5CoO_{26,}$ and $La_{10}Si_5CoO_{26.5}$, or on the La site, $La_8BaCoSi_6O_{26}$. The samples were prepared from the starting materials La_2O_3, SiO_2, and Co_3O_4. Stoichiometric mixtures were intimately ground and heated for 12 hours at 1350ºC with a second firing at 1400ºC, except for $La_8BaCoSi_6O_{26}$, which was calcined at 1250ºC and again at 1300ºC before final annealing at 1350ºC. Between firings the samples were reground to ensure homogeneous reaction, with phase purity being ascertained using a Seifert 3003TT powder X-ray diffractometer.

Conductivity measurements were performed using AC impedance spectroscopy (Hewlett Packard 4192A Impedance Analyser). Samples for measurement were pressed into 13mm diameter pellets and fired for 2 hours. For $La_{9.66}Si_5CoO_{26}$, $La_{9.83}Si_{4.5}Co_{1.5}O_{26}$ and $La_{10}Si_5CoO_{26.5}$ a sintering temperature of 1625ºC was used to obtain dense pellets, whilst $La_8BaCoSi_6O_{26}$ was fired at 1300ºC. Pt electrodes were then affixed to the pellets using Pt paste and the pellet fired again, at 850ºC, for 30 mins to give good electrical contact between sample and electrode.

Time of flight neutron diffraction data were recorded at the ISIS facility, Rutherford Appleton Laboratory. Two instruments were used: HRPD and POLARIS. HRPD was used for the samples $La_{9.66}Si_5CoO_{26}$, $La_{9.83}Si_{4.5}Co_{1.5}O_{26}$ and $La_{10}Si_5CoO_{26.5,}$ whilst for $La_{9.83}Si_{4.5}Co_{1.5}Co_{1.5}O_{26}$ POLARIS was employed. All structural refinements employed the GSAS suite of Rietveld refinement software [21].

Extended X-ray absorption spectroscopy (EXAFS) and X-ray absorption near edge structure (XANES) measurements were performed using the 2GeV Daresbury Synchrotron Radiation Source. The EXAFS experiment measures the oscillations beyond a chosen X-ray absorption edge arising from interference of an ejected photoelectron wave with the fraction of the wave backscattered from neighbours of the absorbing atom. Fourier transform of this oscillatory fine structure yields a radial distribution in real space with peaks corresponding to the electron density surrounding the absorbing atom. Analysis of this can reveal information relating to the local environment of chosen atom types.

Data were collected using two instruments: Si-K edge (1.84keV) EXAFS was performed using station 3.4, whilst Co-K edge (7.71keV) EXAFS and XANES data were collected using station 7.1. Twin single crystal monochromators (InSb(111) for station 3.4, Si(111) for station 7.1) were used for wavelength selection. Due to absorption effects, all data for our samples were collected in fluorescence mode, whilst Co-K edge XANES data for the reference samples $CoTiO_3$, $YSr_2Cu_2CoO_7$ and $LaCoO_3$ were collected in transmission. Several scans were performed for each sample and the thus obtained data summed to reduce statistical noise. Data analysis was performed using the Daresbury suite of EXAFS software: EXCALIB, EXSPLINE and EXCURV98. For the Si and Co edge data of $La_{9.66}Si_5CoO_{26}$, only the first shell M-O was fitted, due to the complexity of the structure beyond the first shell. For the Co edge data of $La_8BaCoSi_6O_{26}$ only shells out to 3.4Å were fitted, as increasing structural complexity again rendered the addition of further shells statistically invalid.

3. Results and discussion

The samples $La_{9.83}Si_{4.5}Co_{1.5}Co_{1.5}O_{26}$, $La_{9.66}Si_5CoO_{26,}$ $La_{10}Si_5CoO_{26.5}$, and $La_8BaCoSi_6O_{26}$ were successfully prepared. Attempts were made to incorporate further Co onto the La site, and so prepare $La_8Co_2Si_6O_{26}$, however impurities were observed for such a sample.

As previously reported [7] the conductivities for samples doped with Co on the Si site were high ($\sigma_{500°C}$ = 2.95 x 10^{-3}Scm^{-1}, 1.5 x 10^{-3} Scm^{-1}, and 2.47 x 10^{-3} Scm^{-1} for $La_{9.66}Si_5CoO_{26,}$ $La_{9.83}Si_{4.5}Co_{1.5}Co_{1.5}O_{26}$, $La_{10}Si_5CoO_{26.5}$ respectively). In contrast the conductivity of the sample with Co doped onto the La site, $La_8BaCoSi_6O_{26}$, was low ($\sigma_{500°C}$= 9.2 x 10^{-7} Scm^{-1}). This sample is nominally stoichiometric on both the rare

earth and Si sites, and so the low conductivity is consistent with previous results that fully stoichiometric samples, e.g. $La_8M_2Si_6O_{26}$ (M=alkaline earth) exhibit poor conductivities [6,9,20].

3.1 – Structural Determination

As apatite systems have been reported to exhibit a variety of space groups, depending on ordering effects, initial Rietveld analysis of the diffraction data focussed on the determination of the appropriate symmetry for our systems. In accordance with previous studies on apatite type systems, three space groups were examined: $P6_3/m$, $P6_3$ and P-3, with the assignment being based on the residual R-factors.

It has been found in previous studies that conductivity in these systems is strongly correlated with evidence of oxygen disorder along the [0,0,z] channels. This is manifested in high Anisotropic Thermal Displacement Parameters (ADP's) for the channel O5 oxygen site, particularly for U_{33}, which corresponds to displacement along the channel c-direction [17]. In our recent investigation of the $La_{10-y}Si_{6-x}Ga_xO_{26+z}$ system [18] we also found high ADP's for the tetrahedral SiO_4 oxygen positions, and evidence of localised distortions of the tetrahedra. Similar effects were also observed for $La_{9.33}Si_6O_{26}$ which has no Si-site dopants [6].

Initial refinements of the $La_{9.83}Si_{4.5}Co_{1.5}O_{26}$ data gave good agreement between our starting model and observed powder pattern, and we were able to assign the space group $P6_3$ to the system. For the compositions $La_{9.66}Si_5CoO_{26}$ and $La_{10}Si_5CoO_{26.5}$, however, there was poor agreement between observed and calculated peak intensities

for all chosen symmetries. Close inspection of the diffraction patterns showed that peaks of index hk0 were sharp, whilst peaks of index l>1 showed broadening. Particularly broadened were peaks of high l and low hk values (124/214, 125/215 etc), and the only clearly observable 00l peak, 004, showed pronounced broadening. To account for this an additional lorentzian-type peak profile parameter was included in the refinement, with the broadening vector set along the c-axis. With this parameter included in the refinement, it was again found that $P6_3$ was the most statistically valid space group. It should be noted that the $La_{10}Si_5CoO_{26.5}$ data was refined as the non-electroneutral composition $La_{10}Si_5CoO_{26}$. Initial attempts to locate the interstitial 0.5 oxygen using Fourier DELF maps yielded no obvious positions of unfitted scattering, and so models including an additional channel-edge "O7" type position, as predicted by our modelling studies, were investigated. A stable site located at (0.0509, 0.2371, 0.8241) was found, and an overall stoichiometry of $La_{10}Si_5CoO_{26.6}$ calculated, but as the refinements showed no statistical improvement in fit we were unable to justify its inclusion in our final model. For all other samples, no anion non-stoichiometry was found, nor were any compositions found to deviate from expected cation stoichiometry. In accordance with previous experimental observations, and predictions from modelling, the 6c La site was found to be fully occupied by La, with dopants and La non-stoichiometry preferring the ±[2/3,1/3,z] channel positions.

For the composition $La_8BaCoSi_6O_{26}$ we again initially assigned space group $P6_3$, rather than $P6_3/m$ which is usually exhibited by fully stoichiometric systems. Using this symmetry Co and Ba were suggested to order along the ±[2/3,1/3,z] La channels, with La taking equal occupation of both channel positions. However, investigation of the respective interatomic bond distances for the Ba and Co containing sites showed

little difference, despite the large difference in ionic radii for Ba^{2+} and Co^{2+} (1.49Å vs 0.79Å for octahedral coordination). Subsequent calculation of Bond Valence Sums for the system indicated that no model of cation ordering was consistent with the observed bond distances, and so $P6_3/m$ symmetry was again investigated. This assignment removes the possibility of cation ordering, as the two 6-fold ±(2/3,1/3,z) channel positions in $P6_3$ become a single 12-fold position with $P6_3/m$. With this symmetry choice, a weighted mean Bond Valence Sum of 2.56 was calculated for this site. This agrees well with the expected value of 2.5 for our chosen structural model, in which Ba and Co dopants are present in addition to La. Space group $P6_3/m$ was thus assigned.

Our final refined structure parameters and Rietveld residual agreement values are presented in tables 1-4, and fitted profiles for $La_{9.66}Si_5CoO_{26}$ and $La_8BaCoSi_6O_{26}$ are shown in figures 2 and 3. From our results, several points are worthy of discussion:

Our work shows that Co is seen to dope onto both the nine-coordinate channel La positions and onto the tetrahedral Si site depending on the starting composition employed. Our XANES results (see below) indicate that La is substituted by Co^{2+}, whilst Si is substituted by Co^{3+}, as would be expected from ionic size considerations and sample stoichiometry.

In accord with our previous studies on related systems [6,18], an ordering of the La vacancies is observed for the $La_{9.83}Si_{4.5}Co_{1.5}O_{26}$ and $La_{9.66}Si_5CoO_{26}$ compositions, in which the distribution of these vacancies in the La positions within the structure is

not random, but concentrated on the ±(2/3,1/3,z) positions whilst La fully occupies the other position.

Analogously with our previous studies on the $La_{10-x}Si_{6-y}Ga_yO_{26+z}$ system, we find that for samples with Co doped onto the Si sites, both the unit cell c-axis and Si/Co-O bond distances increase with increased Co content, due to the larger size of the Co^{3+} dopant. A similar lengthening of the c-axis is observed for the $La_{10}Si_5CoO_{26.5}$ composition, due to the increased oxygen content. In contrast, the doping of Co onto the La site in $La_8BaCoSi_6O_{26}$ causes a general contraction of the unit cell, as expected from the smaller size of Co^{2+} compared to La^{3+}.

High values were obtained for the oxygen Anisotropic Displacement Parameters (ADP's), with the O(3) and O(5) positions in particular exhibiting unrealistically large values (tables 1b). Significant distortion of the SiO_4 tetrahedra is also observed for the $La_{9.66}Si_5CoO_{26}$ and $La_{10}Si_5CoO_{26.5}$ compositions, with a long Si-O(4) bond being displayed. A high level of static disorder of this sort is common even for undoped apatite systems, where it is suggestive of the existence of "O7" type interstitials as predicted by our modelling studies, and found experimentally by Kharton et al [16] and Leon-Reina et al [15]. Formal inclusion of such sites in diffraction data analysis is difficult however, as site occupancy is low and, as found in both this work and by Leon-Reina et al, the stable interstitial site lies ~1Å from the silicate substructure, requiring local relaxation of the structure around the site, which is not possible to model accurately with diffraction methods. With occupancy of the silicon site by the larger cobalt cation in our systems, the uncertainty in silicate oxygen positions is already significant, and a very high level of observed disorder is expected

in this area of the structure. This explains why no improvement in R-factors was achieved by the inclusion of additional oxygen sites at the channel periphery, even though they may indeed be present.

The observed peak broadening provides further evidence of such disorder, being very similar to that reported previously for $La_{9.33}Ge_6O_{26}$ [17] and for the $Cd_{5-x/2}(VO_4)_3I_{1-x}$ and $Cd_{5-x/2}(PO_4)Br_{1-x}$ systems [17,22,23]. For the latter, electron diffraction patterns showed highly structured diffuse scattering along the c-direction. It was postulated that for these systems the effect arises from a displacive distortion of either the (0,0,z) Br or ±(2/3,1/3,z) Cd positions, leading to a different c-directional periodicity for these positions than for the host structure. Considering the relative thermal parameters for the La and O sites in our systems, it seems most likely that the effect arises from a distortion along the O(5) channels. It is apparent that this is only observed for the systems in which Co is substituted on the Si-site (its apparent absence in the $La_{9.83}Si_{4.5}Co_{1.5}O_{26}$ data is attributed to the lower resolution of the Polaris instrument), and that it is observed for both $La_{9.66}Si_5CoO_{26}$ and $La_{10}Si_5CoO_{26.5}$ compositions. Also of note is the fact that such peak broadening is not observed in HRPD data obtained for the equivalent Ga doped systems, despite the similarity in ion size and charge. This does not preclude the existence of such distortions in the Ga systems [18], but rather indicates that the forces between O(5) channels which drive the ordering of such displacements are stronger for the Co systems. The presence of this ordering in both the cation deficient $La_{9.66}Si_5CoO_{26}$ and the fully cation stoichiometric $La_{10}Si_5CoO_{26.5}$ sample also suggests that the distortion is not driven by ordering of vacant La sites in the ±[2/3,1/3,z] channels, but rather of the oxygen.

Another interesting feature from this work is that for $La_8BaCoSi_6O_{26}$, U_{33} for the channel oxygen is high (8.03 $Å^2$, table 3), and yet the conductivity is low. The low conductivity is consistent with previous results that for high conductivity in these apatite systems, nonstoichiometry in the form of cation vacancies and/or oxygen excess is required, however the high value of U_{33} might suggest a high conductivity should be observed. Thus arguments that the high conductivity in apatite systems can be related to the high U_{33} for the channel oxygen seem to be simplistic and other features, such as the silicate network as predicted by modelling studies [13,14], must play a key role.

3.2 – XANES and EXAFS

As diffraction techniques can only give information relating to the structural average, we have used X-ray absorption spectroscopy to examine the local structure for individual sites in our materials. For our studies we have chosen to investigate the changes in local structure upon doping both Co for Si and Co for La. The objective of the experiments were threefold. Firstly to demonstrate conclusively that Co can be doped onto both Si and La sites according to our chosen stoichiometries, secondly to determine the oxidation state of the Co dopant, and finally to relate any changes in local structure with the disorder displayed from the neutron diffraction data.

The Co-k edge positions calculated from XANES spectra of our compositions are presented in table 5, along with those for three standards, $CoTiO_3$, $YSr_2Cu_2CoO_7$ and $LaCoO_3$. These respectively represent octahedral Co^{2+}, tetrahedral Co^{3+} and octahedral Co^{3+}. From edge positions alone we were able to confirm the Co

environments for $La_8BaCoSi_6O_{26}$ and $La_{9.66}Si_5CoO_{26}$ as octahedral Co^{2+} and tetrahedral Co^{3+} respectively. Analysis of the spectra (figures 4a and 4b) confirms this assignment, with $La_{9.66}Si_5CoO_{26}$ and $YSr_2Cu_2CoO_7$ sharing a strong pre-edge and $La_8BaCoSi_6O_{26}$ showing an almost identical spectra to $CoTiO_3$. This latter assignment is highlighted by the strong structural distortion seen from the Co EXAFS analysis, in which the local site coordination is lowered from 9 to 6.

For doping on the Si position, EXAFS data for both dopant and Si edges are presented, although due to difficulties with sample alignment, the quality of Si-edge data were found to be inferior to that of the Co edge. This resulted in slightly low Debye Waller values being obtained for Si edge data. For doping on the La position, only the Co dopant edge data are presented. We note that the La-edge EXAFS is too complex to analyse, due the co-occupation of two distinct crystallographic sites in the structure by La.

The final fitted parameters for our EXAFS investigation of the Si site local structure in $La_{9.66}Si_5CoO_{26}$ are presented in table 6a, with fitted data shown in figures 5-6. Visual inspection of the spectra confirms the expectation that Co^{3+} dopes onto the Si site. Data analysis confirmed a 4 coordinate environment for both edges. First shell Si-O bond distances of ~1.58Å were obtained, whilst for the Co edge a value of 1.85Å was calculated, indicating a considerable difference in local structure around the dopant species. This agrees well with the increase in site size that would be expected from the relative ionic radii considerations, and also supports the origin of the structural disorder exhibited in the neutron diffraction data. There is thus a marked difference in the local structure surrounding the Si and dopant species. This is in

accord with the increase in site size that would be expected from the relative ionic radii. Due to the complexity of the structure beyond the first shell, and the poor resolution of the second shell in all data, no structurally sensible information could be obtained for shells other than the first, and so it was chosen to leave further shells unfitted.

Visual inspection of the fourier transform data collected for the Co-K edge of $La_8CoBaSi_6O_{26}$ (figure 11) clearly shows a very different shell structure to that seen for the Si-site local environment, confirming substitution of Co^{2+} onto the lanthanum sublattice, in accord with the calculated energetics. However, the choice of starting model for analysis was difficult, as the 1st and 2nd shells do not correspond well to the reference crystallographic data for either La site. Our starting models were thus derived with reference to our preliminary modelling studies [24].

Our final fitted model is presented in table 6. We note that only shells out to 3.4Å were fitted, as increasing structural complexity and poor data resolution made the addition of further shells statistically invalid. Substitution onto the La(1) sublattice was confirmed, but with considerable distortion of the local structure: the Co^{2+} dopant assumes a strong 6-coordination, with interatomic distances to the first five shells all being shortened by ~0.4Å relative to the crystallographic "average". For the M-O(2) distance of the first shell this represents a very significant contraction of >15%, and accords with expectations based upon the relative ionic radii for La^{3+} and the Co^{2+} dopant (1.17Å and 0.79Å respectively). We note that the six-coordinate first shell exhibits slightly high Debye-Waller factors. This arises because the shell is actually comprised of two three-coordinate shells at slightly different radial distances (table 6).

Although the data does not allow resolution of the shell structure at longer distances, it is reasonable to assume that the shortening of the M-Si distances is also indicative of an effect on the SiO_4 unit as a whole, "pulling" the unit away from the [0,0,z] O(5) channel. As the SiO_4 units show faces to both the La and O(5) structural channels, it can be suggested that doping on the La channel site positions can thus have a significant effect on the periphery of the O(5) channels, along which oxygen migration is predicted to occur. It is also notable that this distortion occurs very close to the low energy "O7" interstitial position predicted from our previous simulation studies [13,14], and so may influence the formation/migration of such interstitial oxygen defects.

4. Conclusions

The results presented here demonstrate that Co can be doped onto both the Si and La sites in the apatite structure, with the data suggesting that it substitutes onto the Si site as Co^{3+}, and onto the La site as Co^{2+}.

The structural data collected using the high resolution diffractometer, HRPD, showed significant complexities, with evidence for anisotropic peak broadening for samples with Co on the Si site. This anisotropic peak broadening has been attributed to an incommensurate ordering of the oxygens within the channels.

The EXAFS data confirms that the doping on both Si and La sites causes significant structural changes, which could have an important effect on the conduction in these materials.

5. Acknowledgements

The authors would like to thank EPSRC for funding this work. We would also like to express thanks to ISIS and Daresbury SRS facilities, for neutron and EXAFS beam time and to Lorrie Murphy and Kevin Knight for their respective help in the EXAFS and neutron data collection and analysis.

References

[1] S. Nakayama, T. Kagayama, H. Aono and Y. Sadoaka, *J. Mater. Chem.*, 1995, **5**, 1801
[2] S. Nakayama and M. Sakamoto, J. Eur. Ceram. Soc., 1998, **18**, 1413
[3] H. Arikawa, N. Nishiguchi, T. Ishihara and Y. Takita. *Solid State Ionics*, 2000, **136-137**, 31
[4] S. Nakayama, M. Sakamoto, M. Higuchi, K. Kodaira, M. Sato, S. Kakita, T. Suzuki and K. Itoh. *J. Eur. Ceram. Soc*. 1999, **19**, 507
[5] S. Nakayama, M. Sakamoto, M. Highchi and K. Kodaira. *J. Mater. Sci. Lett.* 2000, **19**, 91
[6] J.E.H. Sansom, D. Richings and P.R. Slater. *Solid State Ionics.* 2001, **139**, 205
[7] J. MacFarlane, S. Barth, M.Swaffer, J.E.H. Sansom and P.R. Slater, *Ionics*, 2002, **8**, 149
[8] J.E.H. Sansom and P.R. Slater, *Proc. 5th Euro. SOFC Forum*, 2002,
[9] E.J. Abram, D.C. Sinclair and A.R. West, *J. Mater. Chem*. 2001, **11**, 1978
[10] J.E.H. Sansom, A. Najib and P.R. Slater. *Solid State Ionics.* In Press
[11] S. Tao and J.T.S. Irvine, *Mater Res. Bull*. 2001, **36**, 1245
[12] L. León-Reina, M.C. Martín-Sedeño, E.R. Losilla, A. Cabeza, M. Martínez-Lara, S. Bruque, F.M.B. Marques, D.V. Sheptyakov and M.A.G. Aranda. *Chem. Mater*. 2003, **15**, 2099
[13] M.S. Islam. J.R.Tolchard and P.R. Slater. *Chem Commun.* 2003, 1486
[14] J.R. Tolchard, M. S. Islam and P.R. Slater. *J. Mater. Chem.* 2003, **13**, 1956
[15] L. León-Reina, E.R Losilla, M. Martínez-Lara, S. Bruque and M.A.G Aranda. *J. Mater. Chem*, 2004, **14**, 1142
[16] V.V. Kharton, A.L. Shaula, M.V. Patrakeev, J.C. Waerenborgh, D.P. Rojas, N.P. Vyshatko, E.V Tsipis, A.A. Yaremchenko and F.M.B. Marques. *J. Electrochem. Soc. 2004, **151**, A1236*
[17] P. Berastegui, S. Hull, F.J. García García and J. Grins. *J. Solid State Chem.*2002, **168**, 294
[18] J.E.H. Sansom, J.R. Tolchard, P.R. Slater and M.S. Islam. *Solid State Ionics*. 2004, **167**, 17
[19] A. Najib, J.E.H. Sansom, J.R. Tolchard, P.R. Slater and M.S. Islam. *Dalton Trans*, 3106-3109, 2004.
[20] P.R. Slater and J.E.H. Sansom. *Solid State Phenomena.* 2003, **90-91**, 195
[21] A.C. Larson, R.B. Von Dreele. *Los Alamos National Laboratory, Report*. No LA-UR-86-748, (1987).
[22] P. Alberius-Henning, M. Moustiakimov and S. Lidin. *J. Solid State Chem*. 2000, **150**, 154
[23] A. G. Christy, P. Alberius-Henning and S. Lidin. *J. Solid State Chem*. 2001, **156**, 88
[24] J. Tolchard, P.R. Slater, M.S. Islam. *Manuscript in preparation*

Figure 1 – The structure of the apatite-type oxide, $M_{10}X_6O_{26}$, showing the XO_4 tetrahedra, M(1)/(2) channels at [2/3,1/3,z] and the O(5) channels at [0,0,z]

Figure 2 – Fitted neutron diffraction data for $La_{9.66}CoSi_5O_{26}$

Figure 3 – Fitted neutron diffraction data for $La_8BaCoSi_6O_{26}$

Figure 4 – Co K-edge XANES spectra. (a) $La_8BaCoSi_6O_{26}$ and $CoTiO_3$. (b) $La_{9.66}Si_5CoO_{26}$ and $YSr_2Cu_2CoO_7$

Figure 5 – Fitted Co K-edge spectra for $La_{9.66}Si_5CoO_{26.}$ (a) EXAFS spectrum. (b) Fourier transform data

Figure 6 – Fitted Si K-edge spectra for $La_{9.66}Si_5CoO_{26}$ (a) EXAFS spectrum. (b) Fourier transform data

Figure 7 – Fitted Co K-edge spectra for $La_8BaCoSi_6O_{26}$. (a) EXAFS spectrum. (b) Fourier transform data

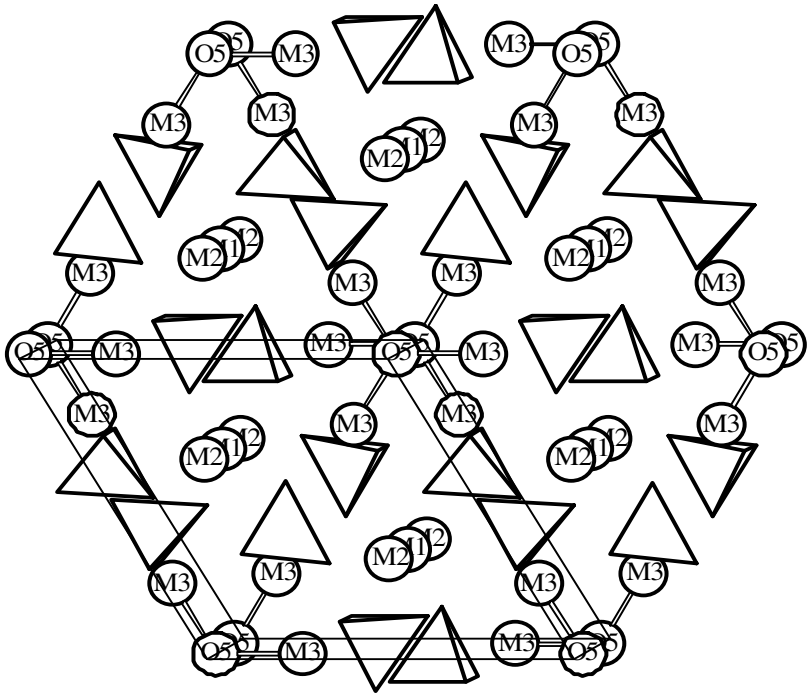
O5
M3
M2
I1
I2

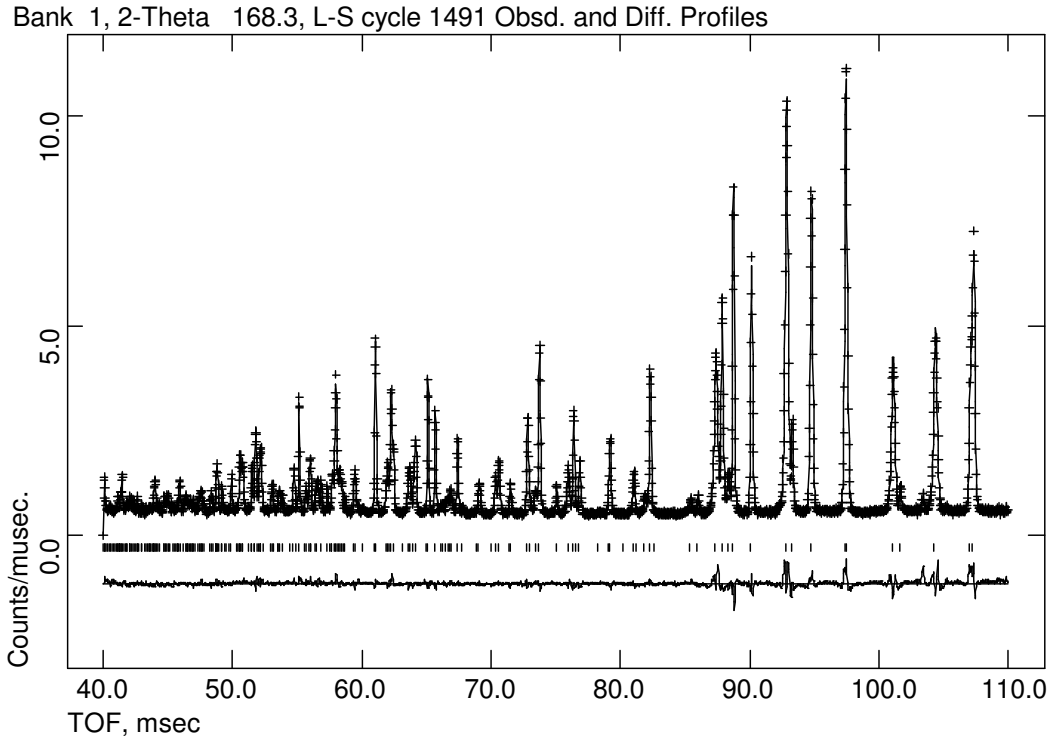
Bank 1, 2-Theta 168.3, L-S cycle 1491 Obsd. and Diff. Profiles
Counts/musec.
10.0
5.0
0.0
40.0
50.0
60.0
70.0
80.0
90.0
100.0
110.0
TOF, msec

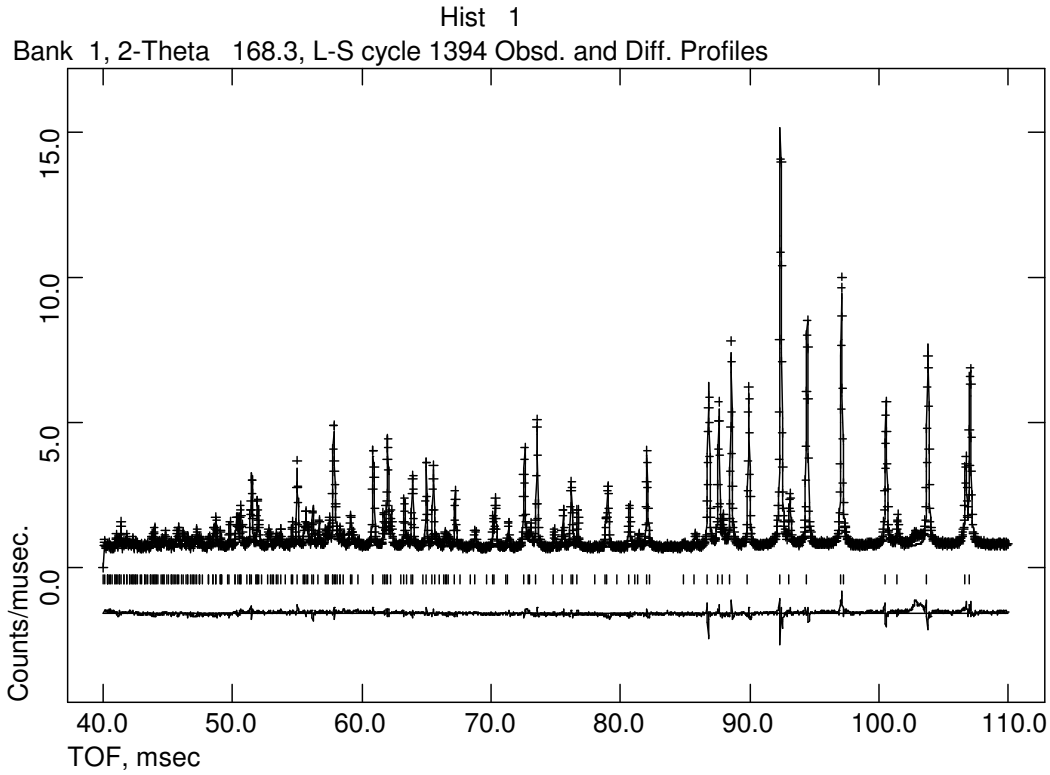
Hist 1
Bank 1, 2-Theta 168.3, L-S cycle 1394 Obsd. and Diff. Profiles
Counts/musec.
0.0
5.0
10.0
15.0
40.0
50.0
60.0
70.0
80.0
90.0
100.0
110.0
TOF, msec

a)

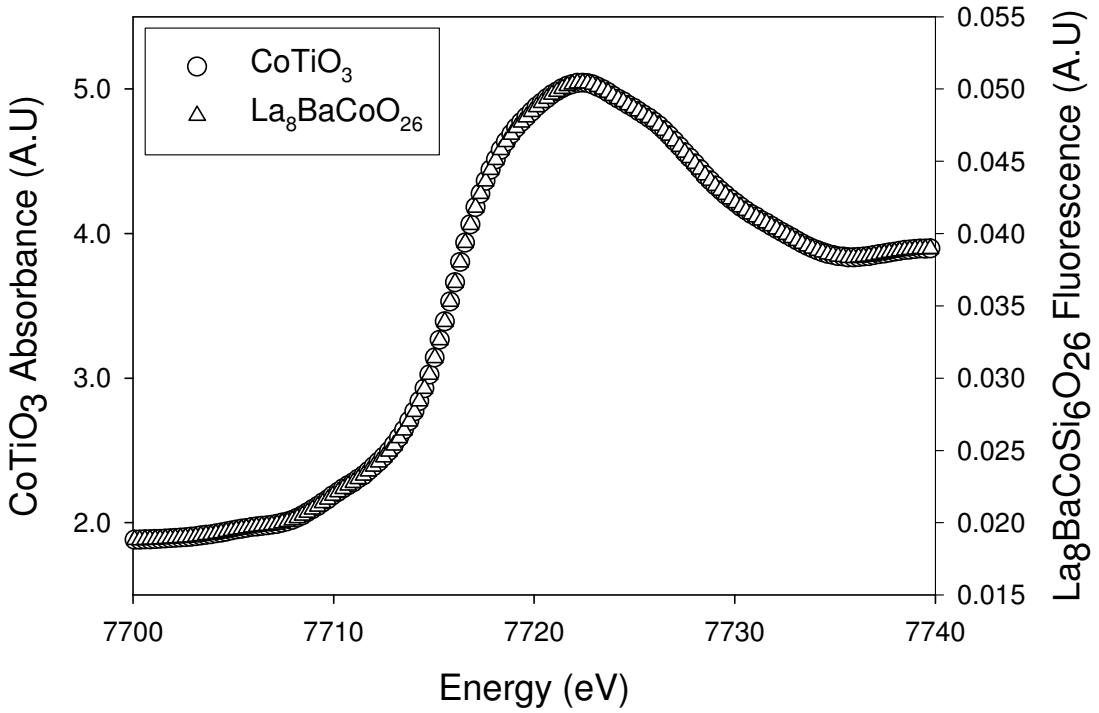
CoTiO3
La8BaCoO26
CoTiO3 Absorbance (A.U)
La8BaCoSi6O26 Fluorescence (A.U)
Energy (eV)
5.0
4.0
3.0
2.0
0.055
0.050
0.045
0.040
0.035
0.030
0.025
0.020
0.015
7700
7710
7720
7730
7740

b)

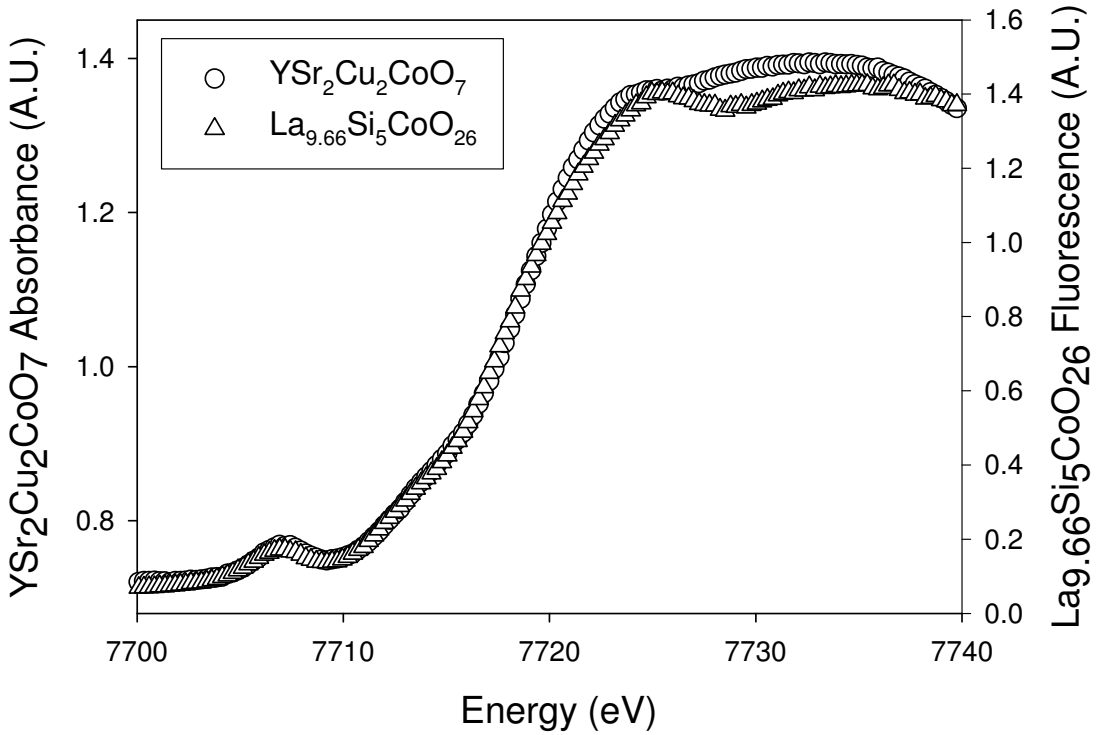
YSr2Cu2CoO7
La9.66Si5CoO26
YSr2Cu2CoO7 Absorbance (A.U.)
La9.66Si5CoO26 Fluorescence (A.U.)
Energy (eV)
1.4
1.2
1.0
0.8
1.6
1.4
1.2
1.0
0.8
0.6
0.4
0.2
0.0
7700
7710
7720
7730
7740

a)

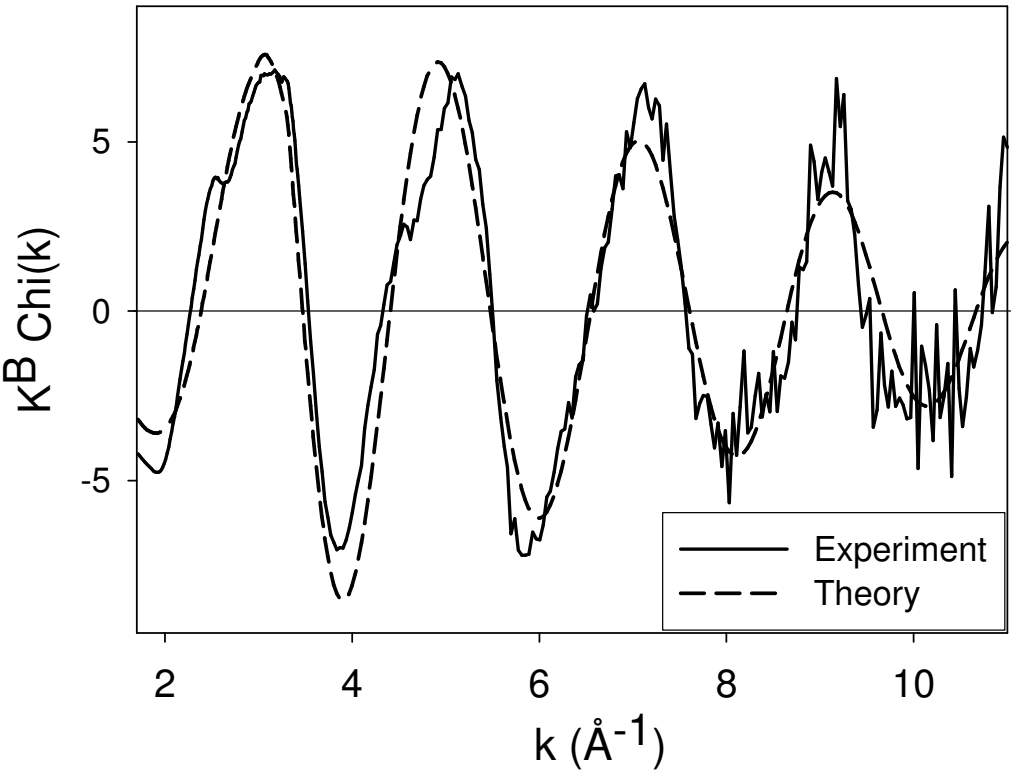
5
0
-5
K^B Chi(k)
2
4
6
8
10
k (Å^-1)
Experiment
Theory

b)

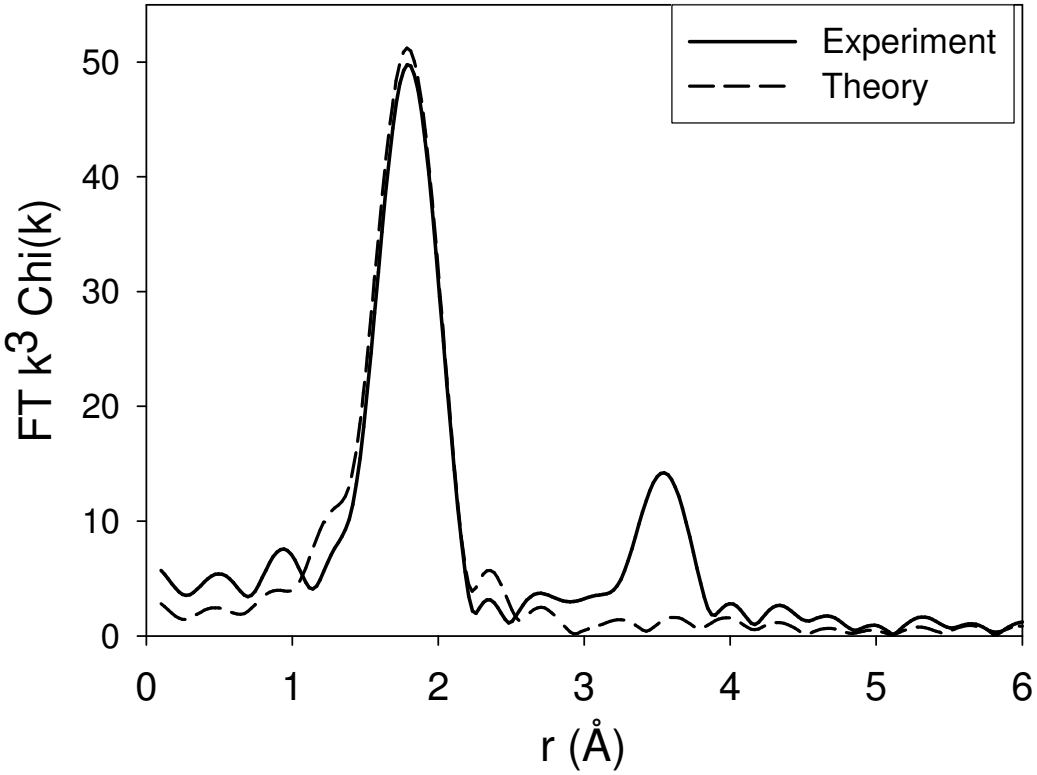
50
40
30
20
10
0
FT k^3 Chi(k)
0
1
2
3
4
5
6
r (Å)
Experiment
Theory

a)

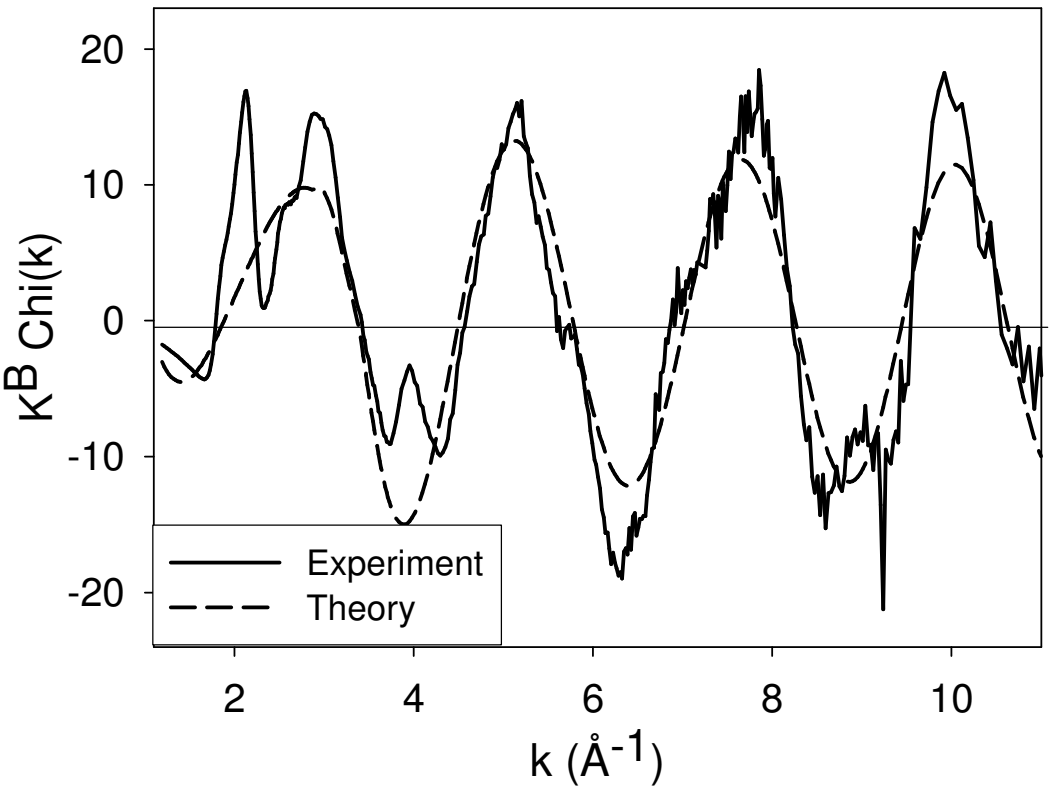
20
10
0
-10
-20
K^B Chi(k)
Experiment
Theory
2
4
6
8
10
k (Å^{-1})

b)

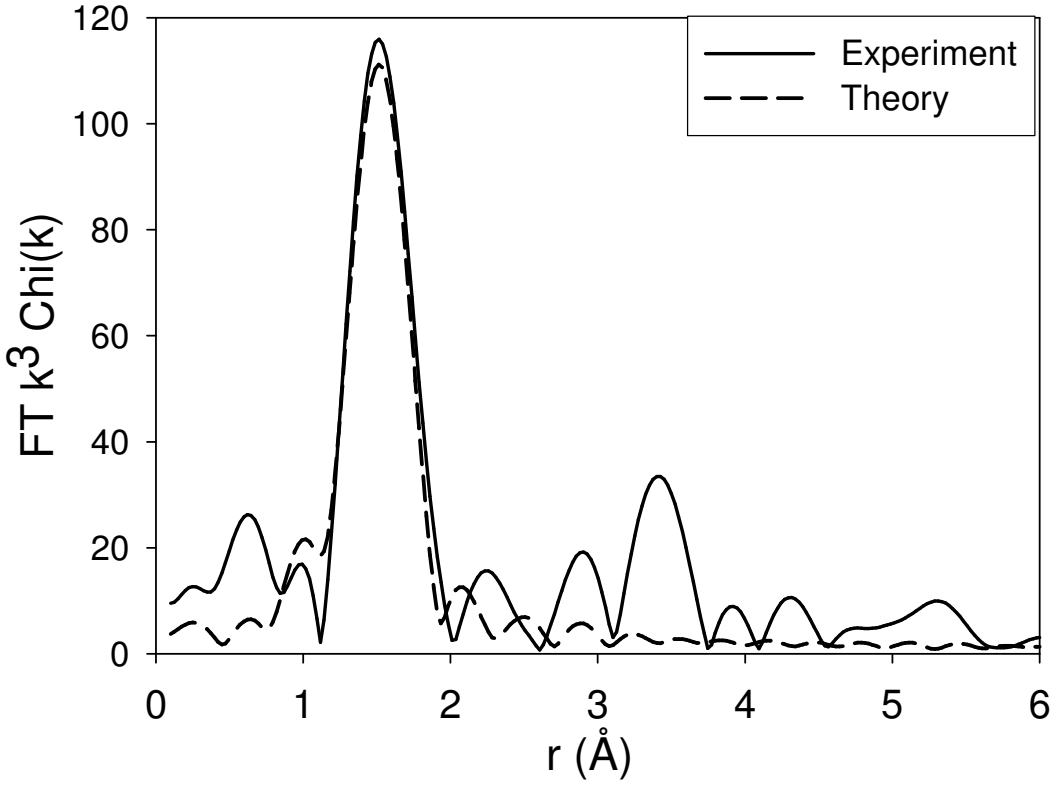
120
100
80
60
40
20
0
FT k^3 Chi(k)
Experiment
Theory
0
1
2
3
4
5
6
r (Å)

a)

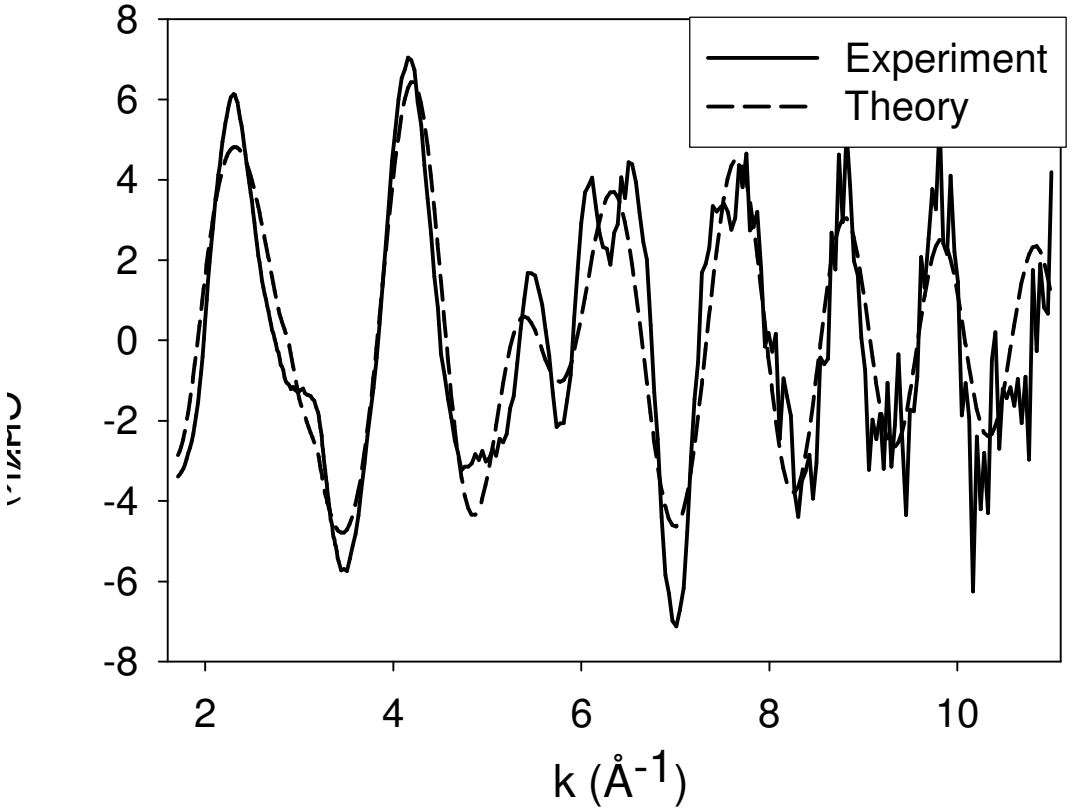
Experiment
Theory
8
6
4
2
0
-2
-4
-6
-8
2
4
6
8
10
k (Å-1)

b)

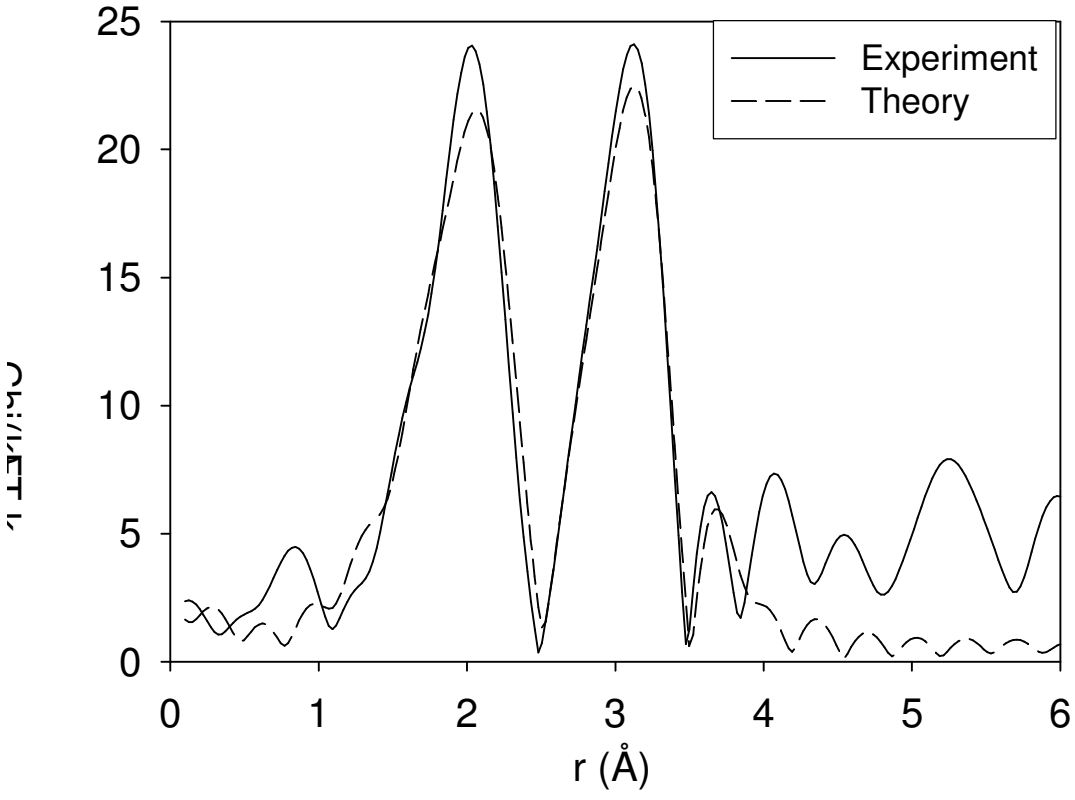
Experiment
Theory
25
20
15
10
5
0
0
1
2
3
4
5
6
r (Å)